THE JOURNAL OF BIOLOGICAL CHEMISTRY
Vol. 275, No. 35, Issue of September 1, pp. 27100–27109, 2000

Printed in U.S.A.

Amyloid β-Peptide-binding Alcohol Dehydrogenase Is a Component of the Cellular Response to Nutritional Stress*

Received for publication, January 4, 2000, and in revised form, June 15, 2000
Published, JBC Papers in Press, June 26, 2000, DOI 10.1074/jbc.M000055200

Shi Du Yan‡§, Yucui Zhu‡, Eric D. Stern‡, Yuying C. Hwang‡, Osamu Hori¶, Satoshi Ogawa¶, Matthew P. Frosch‖, E. Sander Connolly, Jr.‡, Ryan McTaggert‡, David J. Pinsky‡ ‡‡, Steven Clarke§§, David M. Stern‡, and Ravichandran Ramasamy‡**

From the ‡Departments of Pathology, Surgery, Physiology & Cellular Biophysics, Neurosurgery and Medicine, College of Physicians and Surgeons of Columbia University, New York, New York 10032, the ¶Department of Neuroanatomy, Kanazawa Medical University, Kanazawa, Japan, the ‖Center for Neurologic Disease and Department of Pathology, Brigham and Women's Hospital, Boston, Massachusetts 02115, and the §§Department of Chemistry and Biochemistry, UCLA, Los Angeles, California 90095

Amyloid β-peptide-binding alcohol dehydrogenase (ABAD) is a member of the family of short chain dehydrogenase/reductases whose distinctive properties include the capacity to bind amyloid β-peptide and enzymatic activity toward a broad array of substrates including *n*-isopropanol and β-estradiol. In view of the wide substrate specificity of ABAD and its high activity on L-β-hydroxyacyl-CoA derivatives, we asked whether it might also catalyze the oxidation of the ketone body D-3-hydroxybutyrate. This was indeed the case, and oxidation proceeded with K_m of ~4.5 mM and V_{max} of ~4 nmol/min/mg protein. When placed in medium with D-β-hydroxybutyrate as the principal energy substrate, COS cells stably transfected to overexpress wild-type ABAD (COS/wtABAD) better maintained 3-(4,5-dimethylthiazol-2-yl)-2,5-diphenyl tetrazolium bromide reduction, cellular energy charge, and morphologic phenotype compared with COS/vector cells. Using a severe model of metabolic perturbation, transgenic mice with targeted neuronal expression of ABAD subjected to transient middle cerebral artery occlusion showed strokes of smaller volume and lower neurologic deficit scores in parallel with increased brain ATP and decreased lactate, compared with nontransgenic controls. These data suggest that ABAD contributes to the protective response to metabolic stress, especially in the setting of ischemia.

Recent studies of familial Alzheimer's disease have provided support for a close relationship between accumulation of amyloid β-peptide (Aβ),[1] especially the longer form, Aβ(1–42), and development of cerebral dysfunction leading to dementia (1–4). In sporadic Alzheimer's disease, there is an emerging view that decreased clearance of Aβ, possibly mediated by a pathway involving low density lipoprotein receptor-related protein, apoE, and/or α_2-macroglobulin, may contribute to the Aβ-rich environment that disturbs cellular properties (5–8). However, much remains to be learned about the pathways through which Aβ actually induces cellular stress. In the presence of high concentrations of Aβ (micromolar range), generation of oxidants, and changes in calcium homeostasis feed into cell death pathways (9–12). To understand mechanisms that might underlie Aβ-induced cell stress rather than rapid induction of cell death, we have sought cell-associated cofactors capable of magnifying the effects of the amyloid peptide on target cells. We reasoned that such cofactors might be relevant to early phases of Alzheimer's disease when neuronal dysfunction is evolving, but changes are still reversible.

Amyloid β-peptide-binding Alcohol Dehydrogenase (ABAD) is a member of the family of short chain dehydrogenase/reductases (13, 14). It shares features with other members of this family, such as the requirement for a dinucleotide cofactor, nicotinamide adenine dinucleotide (NAD[H]), and a Rossmann-fold structural topology with an invariant sequence, Tyr-*X*-*X*-*X*-Lys, corresponding to residues 168–172 in ABAD, all of which are required for enzymatic activity (15). However, it is distinct from other members of the family in terms of its ability to bind Aβ (13, 14), and its ability to use a broad array of substrates, including linear alcohols, 3-hydroxyacyl-CoA derivatives, and steroids (such as 17β-estradiol) (13, 14, 16–19). In an Aβ-rich environment, ABAD appears to potentiate cell stress induced by the amyloid peptide, as evidenced by increased generation of 4-hydroxynonenal-lysine and malondialdehyde-lysine epitopes and induction of DNA fragmentation (14). Although these observations suggest a "dark side" of ABAD potentially contributing to the pathogenicity of Aβ-induced cellular dysfunction, we reasoned that ABAD is likely to have other properties relevant to normal physiology. Consistent with this concept, inactivation of the *Drosophila* counterpart of ABAD, termed *scully*, resulted in a lethal phenotype with multiple developmental abnormalities (20).

These broad enzymatic properties of ABAD suggested that it might facilitate utilization of ketone bodies by promoting the

* This work was supported by U.S. Public Health Service Grants AG16736, AG00690, AG14103, HL61783, and HL59488, the Surgical Science Research Fund, and the Neuroscience Education Foundation. The costs of publication of this article were defrayed in part by the payment of page charges. This article must therefore be hereby marked "*advertisement*" in accordance with 18 U.S.C. Section 1734 solely to indicate this fact.

§ To whom correspondence should be addressed: Dept. of Pathology, P&S 17-401, College of Physicians & Surgeons of Columbia University, 630 West 168th St., New York, NY 10032. Tel.: 212-305-3958; Fax: 212-305-5337; E-mail: sdy1@columbia.edu.

** Supported by a grant from the American Federation for Aging Research and a Paul Beeson Physician Faculty Scholar in Aging Research award.

‡‡ Recipient of a Clinician Scientist Award from the American Heart Association.

[1] The abbreviations used are: Aβ, amyloid-β peptide; ABAD, Aβ-binding alcohol dehydrogenase; CoA, Coenzyme A; GABA, γ-amino butyric acid; MTT, 3-(4,5-dimethylthiazol-2-yl)-2,5-diphenyl tetrazolium bromide; PD, platelet-derived growth factor B-chain; Tg, transgenic; DMEM, Dulbecco's modified Eagle's medium; HPLC, high pressure liquid chromatography; PDGF, platelet-derived growth factor.

generation of acetyl-CoA to feed into the tricarboxylic acid cycle. This led us to consider a role for ABAD in the cellular response to nutritional/metabolic stress. For example, ketone bodies can reach appreciable concentrations (3–6 mM) in fasted nonhuman primates, both neonatal and infant animals (21), as well as during starvation in normal humans/adult animals (22, 23). Under these conditions, the oxidation of β-hydroxybutyrate becomes the dominant source for energy production in brain (21–23). In the current study, we demonstrate that ABAD does promote utilization of ketone bodies in a cellular environment, probably at the level of both β-hydroxybutyrate. Furthermore, overexpression of ABAD in COS cells, which have low endogenous levels of this enzyme, maintains cellular functions under conditions where β-hydroxybutyrate is the principal energetic substrate. Using NMR to analyze [^{13}C]β-hydroxybutyrate metabolism, ABAD-transfected COS cells displayed increased flux of acetyl-CoA through the tricarboxylic acid cycle. Because ischemia is a severe metabolic stress, a murine stroke model in transgenic mice was employed to determine consequences of overexpressing ABAD in cortical neurons. ABAD transgenic mice demonstrated a protective phenotype with an ~40% reduction in stroke volume and improvement in neurologic deficit scores. Overexpression of ABAD in Tg mice was associated with increased flux of acetyl-CoA through the tricarboxylic acid cycle and increased ATP in cerebral cortex following infusion of β-hydroxybutyrate. These data indicate that expression of ABAD confers a protective phenotype in response to acute metabolic stress, such as that imposed by ischemia, and provide a starting point for further analysis of the properties of ABAD in complex biologic systems.

MATERIALS AND METHODS

Recombinant ABAD and Metabolism of β-Hydroxybutyrate and β-Hydroxybutyryl-CoA—ABAD was produced recombinantly in *Escherichia coli* (BL21) and purified to homogeneity as described (14). D- and L-β-Hydroxybutyrate (sodium salt) and DL-β-hydroxybutyryl-CoA were obtained from Sigma. ABAD oxidation of DL-β-hydroxybutyryl-CoA employed ABAD (330 ng/ml), a range of β-hydroxybutyryl-CoA concentrations (20–1000 μM), and NAD^+ (1.2 mM; Sigma) in 75 mM Tris (pH 10)/75 mM KCl (17). The reaction was run for a total of 10 min at 30 °C under steady-state conditions (24), and the change in NADH absorbance at 340 nm was determined. ABAD oxidation of either D- or L-β-hydroxybutyrate employed 150 μg/ml ABAD, a range of β-hydroxybutyrate concentrations (0.4–25 mM), and 5 mM NAD^+ in 10 mM Tris (pH 7.4)/25 mM NaCl. β-Hydroxybutyrate, NADH, and Tris/NaCl were preincubated for 10 min at 37 °C. Then the enzyme was added, and the reaction was run for a total of 30 min at 30 °C under steady-state conditions as above, except that absorbance at 340 nm was determined (data from the first 10 min were used, when the change in absorbance was linear). Kinetic data were analyzed for Michaelis-Menten by PRISM (Scitech, San Diego, CA) to determine K_m and V_{max}, and lines shown in the figures represent theoretical curves according to kinetic parameters calculated by the program. One unit of enzyme activity was defined as that which converts 1.0 μmol of substrate to product/min.

Generation and Characterization of Stably Transfected COS Cells Expressing ABAD—COS cells (ATCC; 10^5 cells) were transfected with pcDNA3/(human) wild-type ABAD or mutABAD, or pcDNA3 alone (vector) previously linearized with *Sma*I, using LipofectAMINE (14). MutABAD, in which residues 168 (Tyr) and 172 (Lys) in the active site have been replaced by glycine, generating an enzymatically crippled enzyme, has been previously characterized (14). 48 h after transfection, cells were plated at 1:10–1:20 dilution in 100-mm dishes containing 1 mg/ml G418, and, after 1–2 weeks, single clones were isolated, and cells were separated with trypsin, subjected to limiting dilution, and replated in medium containing 1 mg/ml G418 for 2–4 weeks. Cultures were then maintained in DMEM with fetal bovine serum (Life Technologies, Inc.; 10%) and G418 (1 mg/ml), and ABAD expression was characterized as described below. For Northern blotting, total RNA was isolated using Trizol (Life Technologies, Inc.) and run on 1% agarose gels, transferred to nitrocellulose, and hybridized with a full-length ^{32}P-labeled cDNA probe for ABAD (13, 14). For immunoblotting, cell lysates, prepared by directly lysing cell pellets in SDS sample buffer, were subjected to SDS polyacrylamide gel electrophoresis (reduced; 12%) followed by transfer to nitrocellulose. The Blotto procedure was used (25); the first antibody was anti-ABAD peptide IgG (10 μg/ml), and the second antibody was peroxidase-conjugated goat anti-rabbit IgG (1:2000 dilution; Sigma) in the ECL secondary antibody/detection system (Amersham Pharmacia Biotech). Anti-ABAD peptide IgG was prepared and characterized as described previously (13, 14).

Subcellular fractionation of ABAD employed ultracentrifugation of cells disrupted by nitrogen cavitation bomb, as described (14). Following disruption, the lysate was clarified by centrifugation at 10,000 × *g* for 15 min at 4 °C, and the pellet was resuspended in buffer containing 10 mM Tris/HCl (pH 8.0)/1% Nonidet P-40, 150 mM NaCl, 1 mM EDTA, 1 μg/ml aprotonin, and 1 mM phenylmethylsulfonyl fluoride. This material was centrifuged and fractionated through a series of sucrose steps (38, 30, and 20% sucrose prepared in 10 mM HEPES (pH 7.5)/1 mM dithiothreitol). Layered fractions were collected as described (28), and each fraction (5 μg protein/lane) was analyzed by immunoblotting with anti-ABAD peptide IgG. The following markers of subcellular compartments were employed: RAGE for cell membranes (anti-RAGE IgG was prepared as described) (26, 27), GRP78/Bip for endoplasmic reticulum (antibody to GRP78/Bip was obtained from StressGen, Victoria, Canada) (28), and cytochrome *c* for mitochondria (antibody to cytochrome *c* was obtained from StressGen). The mitochondria-rich fraction was also prepared as described by Du *et al.* (29).

^{13}C NMR Spectroscopy—^{13}C NMR spectroscopy is a powerful technique for measuring substrate metabolism in tissue and cell culture (30–38). Addition to culture supernatant or perfusing organs with D-[2,4-^{13}C]3-hydroxybutyrate results in the ^{13}C labeling of tricarboxylic acid cycle intermediates from labeled acetyl CoA (36, 37). Although tricarboxylic acid cycle intermediates are usually present at concentrations too low to be observed by NMR spectroscopy, glutamate, which is present at millimolar concentrations, is in rapid exchange with α-ketoglutarate via aminotransferase reactions. Thus, if ^{13}C-labeled acetyl CoA enters the tricarboxylic acid cycle, the ^{13}C label will be detectable as [^{13}C]glutamate. For experiments with cultured cells (10^7 cells/NMR determination), D-[^{13}C]β-hydroxybutyrate (10 mM) was added to DMEM (without glucose or pyruvate) and dialyzed fetal calf serum (10%). For *in vivo* studies, D-[^{13}C]β-hydroxybutyrate was infused intravenously as follows over 60 min: 0.75 M [^{13}C]β-hydroxybutyrate administered as a bolus (0.05 ml) followed by a constant infusion with a total volume of 1.5 ml (38). At the end of the infusion, brain samples were freeze-clamped under liquid nitrogen and stored at −80 °C. Frozen tissue (sample sizes were 92 ± 6 and 88 ± 11 mg for Tg and non-Tg mice, respectively) was extracted with perchloric acid and neutralized with sodium hydroxide as described (35–37), and homogenates were lyophilized and resuspended in D_2O for NMR analysis. For cell culture studies, culture supernatants and lysates were extracted with perchloric acid followed by neutralization and lyophilization as above.

High resolution carbon spectra were acquired on a Bruker 500 MHz spectrometer, using a 10-mm broad-band probe tuned to 125.77 MHz. Field homogeneity was optimized by shimming on the D_2O lock signal. Spectra were obtained using a 25 KHz sweep width, with 45° pulse and 2-s interpulse delay. Heteronuclear decoupling was performed using a Waltz sequence. Each spectrum represents a total of 17,920 scans. The assignment of ^{13}C resonances was based on previously published studies (33, 34, 36–38). Glutamate peak areas were determined using Bruker NMR software and are expressed as ratios with the summed area of the [2,4-^{13}C]β-hydroxybutyrate peaks. In brain extracts, the area measurements for glutamate, glutamine and γ-amino butyric acid (GABA) are compared with spectra obtained from an external standard solution (0.1 M [^{13}C]acetate) using the same acquisition parameters as above. The ^{13}C NMR spectra of standard solutions of glutamine and GABA were obtained to confirm chemical shifts of these compounds in the brain extracts.

^{1}H NMR Spectroscopy—Water presaturation experiments were acquired on the GE500-MHz spectrometer using a 5-mm inverse detection probe (^{1}H observe, with broad band decoupling capabilities). With a sweep width of 5 KHz, a 45° pulse width, and the carrier frequency set on the H_2O peak for a 1-s presaturation pulse, ^{1}H spectra were obtained for 256 total scans. Presaturation experiments were performed both with and without heteronuclear ^{13}C decoupling (for assessing the fractional enrichment in glutamate), centered at 40 ppm, using a Waltz sequence.

The region between 2.6–2.0 ppm reveals proton resonances from the C-4 of glutamate. Although the proton resonances corresponding to [^{12}C-4]glutamate are resolvable, the ^{1}H satellites corresponding to [^{13}C-4]glutamate are obscured by other nearby peaks. Accordingly, the fractional enrichment of glutamate cannot be determined by measuring the areas of the proton peaks bound to labeled and nonlabeled carbons, as

is the case with lactate (32). However, the enrichment of glutamate C-4 may be determined from the increase in intensity of the C-4 glutamate proton resonances following heteronuclear ^{13}C decoupling, because these resolvable resonances then correspond to the sum of protons from labeled and nonlabeled glutamate (32).

Assays of Cellular Function: MTT Reduction and Measurement of Cellular Energy Charge—Reduction of MTT was studied, and phase contrast micrographs of COS cells were made as described previously (13, 39). Measurement of cellular energy charge was also performed by previous methods (40). In brief, cultured cells previously incubated in D-β-hydroxybutyrate, DMEM without glucose or sodium pyruvate (Life Technologies, Inc.), and dialyzed fetal calf serum (10%; Life Technologies, Inc.) were washed three times in phosphate-buffered saline. Adenine nucleotides were extracted with perchloric acid (1 M) and subjected to centrifugation through a layer of bromododecane. The supernatant was neutralized with potassium hydroxide and subjected to reversed-phase HPLC (Microsorb C18; Rainin Instruments Co., Woburn, MA). The column eluate was monitored at an absorbance of 254 nm, and nucleotide concentration was calculated from the peak area using ChromatoPack CR-4A (Shimadzu Seiki, Kyoto, Japan). At each point the energy charge was calculated as described (41).

Generation and Characterization of ABAD Transgenic Mice—The platelet-derived growth factor (PDGF) B-chain promoter was used to drive overexpression of ABAD in neurons of the central nervous system of Tg mice (42). Transgene constructs were prepared using a previously described vector (43, 44). Briefly, the cytomegalovirus immediate/early promoter was excised from the commercial expression vector pCI (Promega, Madison WI), and replaced with an oligonucleotide polylinker. The PDGF B-chain promoter fragment was mobilized as an *Xba*I fragment (42) and cloned into a unique *Spe*I site designed within the synthetic linker. The full-length human ABAD cDNA was inserted into the *Not*I site of the original polylinker. A 3-kilobase fragment containing the promoter, cDNA, and required other sequences was then excised from the plasmid backbone as *Bam*HI fragment and microinjected mouse $B6CBAF_1/J$ oocytes. The latter were implanted into pseudopregnant females and mated with $B6CBAF_1/J$ males resulting in the generation of four founders. These were used to produce lines, which were backcrossed eight times into the C57BL6 background. Tg PD-ABAD mice were identified by Southern blotting, and expression of the transgene was monitored by Northern and Western blotting and immunostaining. Southern blotting was performed on DNA extracted from mouse tails, and hybridization was performed with ^{32}P-labeled cDNA probe for ABAD. Northern and immunoblotting utilized the same procedures as above, except that tissue was homogenized in the presence of Trizol (RNA) or in lysis buffer (20 mM Tris/HCl (pH 7.4), 1% Triton X-100, 2 mM phenylmethylsulfonylfluoride, 1 mM EDTA, 10 μg/ml aprotonin, 10 μg/ml leupeptin, and 1 ml of buffer/0.5 gm of tissue). Note that immunoblotting and immunostaining of brain tissue from Tg PD-ABAD mice used anti-human ABAD peptide IgG, which appears to be preferentially immunoreactive with human ABAD, the latter encoded by the transgene (13). Immunostaining was performed on 4% paraformaldehyde-embedded sections (6 μm) that were deparaffinized and dehydrated and then stained with rabbit anti-human ABAD peptide IgG (8.5 μg/ml) followed by goat anti-rabbit biotin-conjugated IgG and ExtrAvidin-conjugated with alkaline phosphatase (Biotin ExtrAvidin kit; Sigma).

Murine Stroke Model—Mice (C57BL6/J, male) were subjected to stroke according to previously published procedures (45) and in accordance with guidelines of the American Academy of Accreditation of Laboratory Animal Care. Following anesthesia, the carotid artery was accessed using the operative approach previously described in detail (46), including division/coagulation of the occipital and pterygopalatine arteries to obtain improved visualization and vascular access. A nylon suture was then introduced into the common carotid artery and threaded up the internal carotid artery to occlude the origin of the right middle cerebral artery. Nylon (polyamide) suture material was obtained from United States Surgical Corporation (Norwalk, CT) and consisted of 5.0 nylon/13-mm length for 27–36-g mice and 6.0 nylon/12-mm length for 22–26-g mice. After 45 min of occlusion, the suture was withdrawn to achieve a reperfused model of stroke. Although no vessels were tied off after the suture was removed, the external carotid arterial stump was cauterized to prevent frank hemorrhage. Measurements of *relative cerebral blood flow* were obtained as previously reported (45–48) using a straight laser doppler flow probe placed 2 mm posterior to the bregma and 6 mm to each side of midline using a stereotactic micromanipulator, keeping the angle of the probe perpendicular to the cortical surface. These cerebral blood flow measurements, expressed as the ratio of ipsilateral to contralateral blood flow, were obtained at base line, immediately prior to middle cerebral artery occlusion, 45 min after middle cerebral artery occlusion, and at several time points after withdrawal of the occluding suture.

Measurement of Cerebral Infarction Volumes—After 24 h, animals were euthanized, and their brains were rapidly harvested. Infarct volumes were determined by staining serial cerebral sections with triphenyl tetrazolium chloride and performing computer-based planimetry of the negatively (infarcted) staining areas to calculate infarct volume (using NIH image software).

Neurological Exam—Prior to giving anesthesia, mice were examined for neurological deficit 23 h after reperfusion using a four-tiered grading system; a score of 1 was given if the animal demonstrated normal spontaneous movements, a score of 2 was given if the animal was noted to be turning toward the ipsilateral side, a score of 3 was given if the animal was observed to spin longitudinally (clockwise when viewed from the tail), and a score of 4 was given if the animal was unresponsive to noxious stimuli. This scoring system has been previously described in mice (45–47) and is based upon similar scoring systems used in rats (49). Immunostaining of cerebral cortex following induction of stroke in wild-type mice was performed as described above using a rabbit polyclonal antibody made using purified recombinant murine ABAD as the immunogen. Quantitation of microscopic images was accomplished with the Universal Imaging System

ATP and lactate/pyruvate ratio were determined in cerebral cortex from control mice and from ischemic *versus* nonischemic hemispheres of mice subjected to ischemia (measurements were made 24 h after induction of ischemia). Perchloric acid-extracted cerebral cortex was neutralized with sodium hydroxide, and the ATP in the extract was measured using HPLC techniques (50). Lactate, β-hydroxybutyrate, and pyruvate levels in the neutralized extracts were measured using established assays (51).

RESULTS

ABAD Metabolism of β-Hydroxybutyrate—The broad enzymatic properties of ABAD as an oxidoreductase suggested that it might facilitate cellular utilization of ketone bodies, such as D-β-hydroxybutyrate, a major energetic substrate during nutritional deprivation *in vivo*. First, we tested DL-β-hydroxybutyryl-CoA, a known substrate of bovine liver-derived hydroxyacyl-CoA type II (HADH II)/ABAD (17), with our purified *E. coli*-derived human recombinant ABAD; the reaction fit Michaelis-Menten kinetics with K_m was ~134 μM and V_{max} ~26.3 μmol/min/mg (Fig. 1*A*). The latter result, obtained with a racemic DL mixture of β-hydroxybutyryl-CoA, was similar to that observed previously with the bovine liver HADH II (17). Using the same preparation of recombinant ABAD, we then studied D-β-hydroxybutyrate; the reaction also fit Michaelis-Menten kinetics with a K_m of ~4.5 mM and a V_{max} of ~4 nmol/min/mg (Fig. 1*B*). With the L-form of β-hydroxybutyrate, the K_m was ~1.6 mM and the V_{max} was ~4 nmol/min/mg (Fig. 1*C*). In a purified system, ABAD is clearly more effective with β-hydroxybutyryl-CoA as a substrate (presumably this is the L-form, which is an intermediate in the fatty acid β-oxidation pathway in mitochondria). However, depending on physiological conditions, certain substrates may turn out to be more abundant, such as D-β-hydroxybutyrate during periods of starvation when levels of ketone bodies are elevated and, thus, could become relevant. In fact, plasma levels of β-hydroxybutyrate are reported to reach the millimolar range in animals and humans subjected to nutritional deprivation (21–23). Furthermore, β-hydroxybutyryl CoA is another likely substrate of ABAD in a cellular milieu rich in β-hydroxybutyrate. Thus, ABAD would appear to have the potential to be pivotal for enhancing metabolism of β-hydroxybutyrate.

Characterization of COS Cells Stably Transfected to Overexpress ABAD—COS cells provided a useful model to test our concept that ABAD modulated the cellular response to nutritional stress because of their low endogenous expression of ABAD; low levels of mRNA were present (Fig. 2*A*, *lane 4*) and no antigen was detectable (Fig. 2*B*, *lane 7*) in lysates of wild-type COS cells. Following stable transfection with pcDNA3

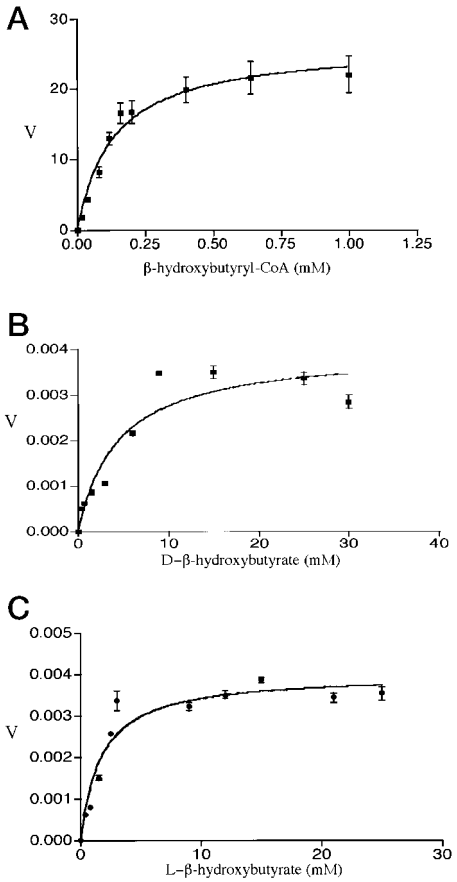

FIG. 1. **ABAD metabolism of β-hydroxybutyrate and β-hydroxybutyryl-CoA.** *A*, ABAD (330 ng/ml) was incubated with the indicated concentration of DL-β-hydroxybutyryl-CoA and NAD^+ (1.2 mM). *B* and *C*, ABAD (150 μg/ml) was incubated with the indicated concentration of D-β-hydroxybutyrate (*B*) or L-β-hydroxybutyrate (*C*) and NAD^+ (5 mM). The velocity (*V*) of the reaction (units/mg of protein) is plotted *versus* added substrate concentration. Details of experimental methods are described in the text. The *line* represents the theoretical curve according to the K_m and V_{max} values calculated by the computer program.

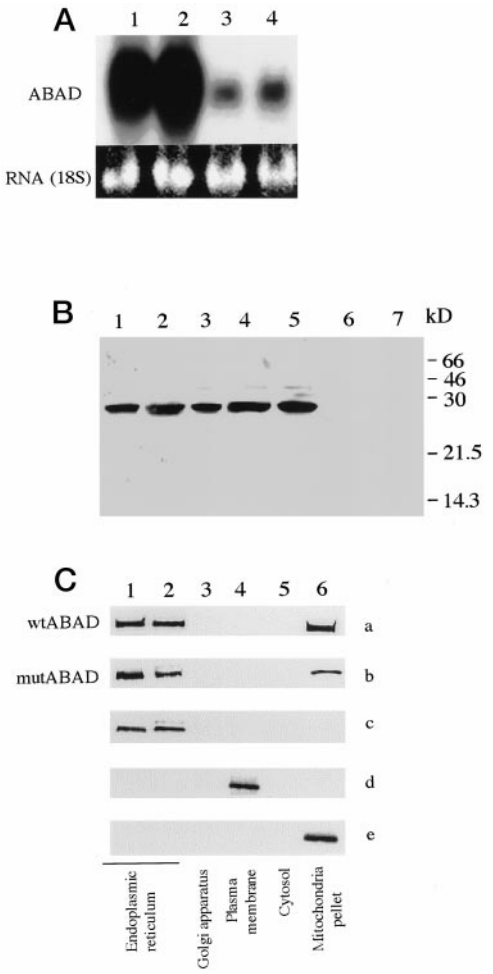

FIG. 2. **Characterization of COS cells stably transfected to overexpress ABAD.** *A*, RNA isolated from stably transfected COS cells, COS/mutABAD (*lane 1*), COS/wtABAD (*lane 2*), COS/vector (*lane 3*), or wild-type COS cells (*lane 4*), was subjected to Northern analysis (30 μg of total RNA was added to each lane). Membranes were hybridized with ^{32}P-labeled cDNA probe for ABAD, and RNA loading was determined based on the intensity of the 18 S ribosomal RNA band on ethidium bromide-stained gels. *B*, protein extracts from stably transfected COS cells (COS/mutABAD, *lanes 1* and *2*; COS/wtABAD, *lanes 3–5*; and COS/vector, *lane 6*) or wild-type COS cells (*lane 7*) were subjected to SDS polyacrylamide gel electrophoresis (12%; reduced; 100 μg of total protein was added to each lane) followed by immunoblotting with anti-ABAD IgG (10 μg/ml). In each case (*lanes 1–5*), protein extracts were obtained from different clones of stable transfectants. The migration of simultaneously run molecular mass standards is shown on the *far right side* of the gel. *C*, stably transfected COS cells (COS/wtABAD, *line a*; COS/mutABAD, *line b*) were subjected to subcellular fractionation by nitrogen bomb cavitation followed by ultracentrifugation through a series of sucrose steps and collection of fractions (1–6). Immunoblotting was performed on fractions using anti-ABAD IgG (*lines a* and *b*), anti-GRP78 IgG (*line c*; as a marker of endoplasmic reticulum), anti-RAGE IgG (*line d*; as a marker of plasma membrane), and anti-cytochrome *c* IgG (*line e*; as a marker of mitochondria).

alone (vector), pcDNA3/wtABAD (encoding wild-type ABAD), or pcDNA3/mutABAD (encoding a mutant form of ABAD devoid of enzymatic activity; Ref. 14), cells were plated at limiting dilution, and clones were prepared. Three types of clones were established: those expressing vector alone (COS/vector), wild-type ABAD (COS/wtABAD), and mutant ABAD (COS/mutABAD). Studies were performed with three representative clones of each type of stably transfected COS cell. Whereas COS/vector cells displayed low levels of ABAD transcripts (Fig. 2*A*, *lane 3*) and antigen (Fig. 2*B*, *lane 6*), comparable with control COS cells, COS/wtABAD cells showed high levels of ABAD mRNA (Fig. 2*A*, *lanes 2*) and antigen (Fig. 2*B*, *lanes 3–5*). Subcellular fractionation studies on COS/wtABAD cells (Fig. 2*C*, *line a*) demonstrated the presence of ABAD both in fractions 1–2 enriched for the endoplasmic reticulum marker GRP78 (Fig. 2*C*, *line c*) and in the mitochondrial pellet (fraction 6) containing cytochrome *c* (Fig. 2*C*, *line e*). Similar experiments performed with COS/mutABAD stable transfectants (Fig. 2*C*, *line b*) displayed high levels of ABAD transcripts (Fig. 2*A*, *lane 1*) and antigen (Fig. 2*B*, *lanes 1* and *2*) in a distribution analogous to that seen in COS/wtABAD cells. These data indicated that in COS/ABAD stable transfectants, the enzyme is present at the same sites previously observed in cells endogenously expressing ABAD or those transiently transfected to overexpress ABAD (13, 14, 16, 19).

ABAD and the Response of COS Cells to Nutritional Stress—In view of ABAD metabolism of D-β-hydroxybutyrate, we tested whether ABAD-transfected COS cells displayed enhanced ability to sustain nutritional stress in an environment where ketone bodies provided the principal energetic source. When COS/vector cells were placed in medium devoid of glucose and supplemented only with dialyzed serum and β-hydroxybutyrate, cellular functions became compromised. In the presence of D-β-hydroxybutyrate (10 mM), reduction of MTT was suppressed by days 4–5 (Fig. 3*A*), and cellular energy charge decreased in parallel (Fig. 3*C*). Phase contrast microscopy showed COS/vector cells, initially with a spread morphology on the growth substrate, to become rounded up and toxic in

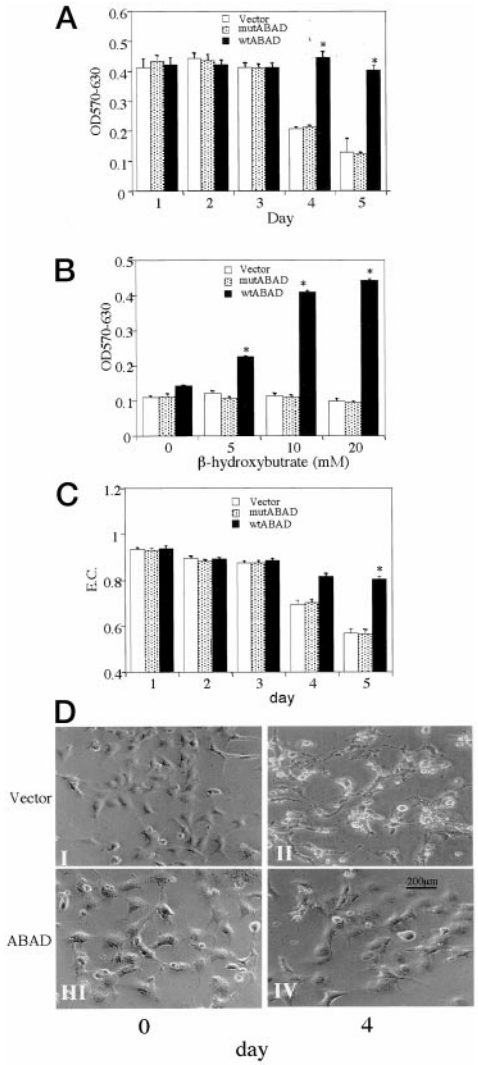

FIG. 3. **Properties of COS/ABAD stable transfectants: effect of D-β-hydroxybutyrate-containing medium.** *A*, COS/wtABAD, COS/mutABAD and COS/vector stable transfectants were placed in DMEM (without glucose or pyruvate) containing D-β-hydroxybutyrate (10 mM) and dialyzed fetal calf serum (10%). MTT reduction was measured on the indicated day. *B*, the experiment was performed with stably transfected COS cells as in *A* for 5 days at the indicated concentration of D-β-hydroxybutyrate. *C*, the experiment was performed with stably transfected COS cells as in *A* with medium containing D-β-hydroxybutyrate (10 mM). On the indicated day, energy charge (*E.C.*) was determined. *D*, COS/ABAD and COS/vector cells maintained in the above medium containing D-β-hydroxybutyrate (10 mM) as above were photographed on day 0 (just after placement in the medium; *panels I* and *III*) or 4 days after incubation under these conditions (*panels II* and *IV*). Experiments were repeated a minimum of three times.

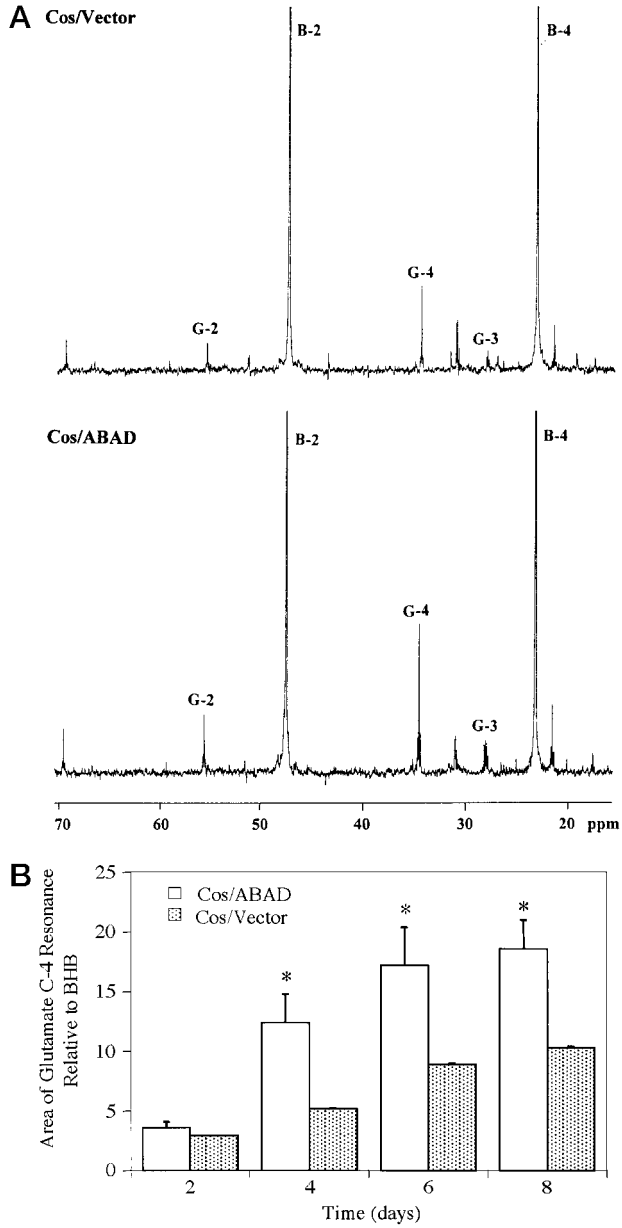

FIG. 4. **The effect of ABAD overexpression on the proton-decoupled ^{13}C NMR spectrum of supernatant from cells perfused with D-[2,4-^{13}C]β-hydroxybutyrate.** *A*, the spectrum from COS/vector (*top panel*) and COS/ABAD (*bottom panel*) cells in DMEM (without glucose or pyruvate) containing D-^{13}C-β-hydroxybutyrate (10 mM) and dialyzed fetal calf serum (10%) displays prominent glutamate peaks. *G-2*, *G-3*, and *G-4* denote the position 2, 3, and 4 carbons of glutamate, respectively; *B-2* and *B-4* denote carbons 2 and 4 of β-hydroxybutyrate. *B*, the effect of ABAD overexpression on the area of glutamate C-4 resonance in the supernatant from studies as in *A*. Values are expressed as the ratio of the areas of the C-4 peak over the summed areas of β-hydroxybutyrate peaks. An *asterisk* indicates that glutamate areas were significantly higher in COS/ABAD than COS/vector cells ($p < 0.03$). The areas are reported as the means ± S.D.

appearance after 4 days under these conditions (Fig. 3*D*, *panels I* and *II*). Similar results were obtained when COS/vector cells were replaced with wild-type COS cells, and the same studies described above were performed (not shown). In contrast, COS/wtABAD cells better maintained MTT reduction (Fig. 3*A*) and cellular energy charge (Fig. 3*C*) in the presence of β-hydroxybutyrate. These changes in cellular properties were parallelled by maintenance of the morphologic phenotype of COS/wtABAD cells, compared with COS/vector transfectants (Fig. 3*D*, *panels III* and *IV*) in the presence of β-hydroxybutyrate. The effect of β-hydroxybutyrate to maintain cellular functions in COS/wtABAD cells was dose-dependent, as shown using the MTT reduction assay, and reached a plateau by 10 mM (Fig. 3*B*). Furthermore, experiments with lower concentrations of β-hydroxybutyrate (≤2.5 mM) displayed less effective maintenance of cellular properties with COS/wtABAD cells (not shown). The requirement for enzymatically intact ABAD (wtABAD) for enhanced survival of COS/wtABAD cells in the presence of β-hydroxybutyrate was shown by experiments performed with COS/mutABAD cells. Although the crippled enzyme (mutABAD) was expressed at similar levels and with a similar subcellular distribution as the wild-type enzyme (the latter in COS/wtABAD cells), COS/mutABAD cells responded to glucose replacement with β-hydroxybutyrate as did COS/vector cells;

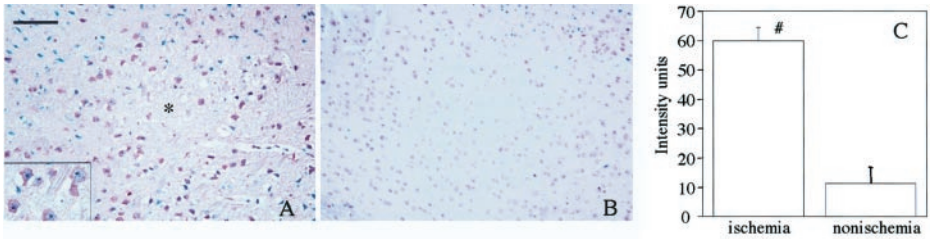

FIG. 5. **Immunohistologic analysis of ABAD in murine cerebral ischemia.** Mice were subjected to the transient middle cerebral artery occlusion model, allowed to recover for 24 h, and then sacrificed. Immunohistologic analysis of formalin-fixed, paraffin-embedded sections of cerebral cortex was performed with rabbit anti-mouse ABAD IgG (20 μg/ml). *A* shows a low power view (*bar*, 10 μm) of the infarcted area (the *asterisk* denotes the center of the infarcted area) displaying sites of ABAD expression, and the *inset* shows the penumbral region. Note the presence of ABAD in neurons. *B* shows the nonischemic hemisphere. *C* shows semiquantitative analysis of immunohistochemical results shown in *A* and *B*. The *asterisk* indicates $p < 0.0001$.

there was a steady decline in MTT reduction and cellular energy charge (Fig. 3, *A* and *C*).

NMR studies were performed on cells incubated with [^{13}C]D-β-hydroxybutyrate (labeled in the C-2 and C-4 positions) to determine the effect of ABAD on the metabolism of the COS/wtABAD transfectants in medium devoid of glucose. ^{13}C-Labeled β-hydroxybutyrate enters the tricarboxylic acid cycle as ^{13}C-2-labeled acetyl-CoA and is metabolized to α-ketoglutarate. Thus, C-4 gets labeled in the first turn of the tricarboxylic acid cycle, and subsequent labeling occurs in the C-3 and C-2 positions. Because α-ketoglutarate is in rapid equilibrium with glutamate, the labeling of [^{13}C]glutamate in the C-4, 3, and 2 positions was observed (Fig. 4*A*). Because the flux of ^{13}C-labeled acetyl-CoA via the tricarboxylic acid cycle is orientation conserved, the labeling of [^{13}C]glutamate is greater in the C-4, compared with the C-3 and C-2, positions. Thus, labeling was evaluated in the C-4 position of glutamate in COS/wtABAD *versus* COS/vector in cell lysates and supernatants. In culture supernatants, NMR data demonstrated greater labeling of the C-4 resonances in glutamate in COS/wtABAD cells, ~2-fold, compared with COS/vector cells (Fig. 4*B*; $p < 0.03$ at days 4, 6, and 8). Glutamine was not detected in supernatants from COS/wtABAD or COS/vector cells. The ^{1}H NMR analysis of these supernatants revealed that the fractional enrichment at glutamate C-4 was 58 ± 3% in COS/wtABAD transfectants compared with 41 ± 2% in COS/vector cells. These data are indicative of increased metabolism of exogenous ^{13}C-labeled β-hydroxybutyrate in COS cells overexpressing ABAD. In contrast, there were no observed differences between fractional enrichment at glutamate C-4 in cell lysates between COS/wtABAD and COS/vector cells, probably because glutamate is rapidly extruded into the medium (glutamine and glutamate levels in cell lysates were the same, comparing COS/wtABAD and COS/vector cells). The ^{13}C and ^{1}H NMR data demonstrate increased exogenous β-hydroxybutyrate utilization in the COS cells overexpressing wtABAD.

Up-regulation of ABAD in Response to Cerebral Ischemia—A severe form of metabolic stress is imposed by cerebral ischemia. Wild-type C57BL6 mice subjected to transient middle cerebral artery occlusion displayed increased levels of ABAD in neurons near the infarcted area (Fig. 5*A*), especially those in the penumbra (Fig. 5*A*, *inset*), compared with the nonischemic hemisphere (Fig. 5*B*), using polyclonal antibody to recombinant mouse ABAD. Image analysis of sections similar to those shown in Fig. 5 (*A* and *B*) demonstrated an ~5-fold increase of ABAD antigen in cortical neurons consequent to stroke (Fig. 5*C*).

Characterization of Tg PD-ABAD Mice—These data with wild-type mice subjected to cerebral ischemia suggested that up-regulation of ABAD might be a component of the response to ischemic stress and led us to make transgenic mice in which ABAD was overexpressed in cortical neurons. Three independent founders of Tg mice in which human ABAD is expressed under control of the human PDGF B-chain promoter have been identified and used to establish transgenic lines (at present backcrossed eight times into the C57BL6 background). Representative mice from each of these transgenic lines showed high levels of transgene activity at both the mRNA (Fig. 6*A*) and protein levels (Fig. 6*B*) in cerebral cortex. Immunoblotting performed on brain subregions from one line of Tg PD-ABAD mice, using an anti-human ABAD peptide antibody that selectively recognizes the human form of the protein, showed increased antigen especially in cerebral cortex and hippocampus, with a smaller increase in cerebellum (Fig. 6*C*). Immunohistochemical staining of ABAD in cerebral cortex confirmed high levels of antigen expression in cortical neurons (Fig. 6*D1*) compared with nontransgenic littermates (Fig. 6*D2*). Semiquantitative analysis of immunohistochemical results using antibody reactive with murine and human ABAD antigen (*i.e.* total ABAD antigen) indicated that there was an ~3.5–4-fold increase in total ABAD antigen in cerebral cortex comparing Tg mice with non-Tg littermate control mice (Fig. 6*D3*). Induction of stroke in transgenic mice further elevated ABAD antigen another 2-fold compared with non-Tg controls (24 h after the ischemic episode; not shown). Growth (height/weight) and reproductive fitness (number and size of litters) was similar between Tg PD-ABAD mice and nontransgenic (non-Tg) controls, and there were no overt neurologic symptoms or other phenotype evident in these mice noted to date.

NMR Analysis of ^{13}C β-Hydroxybutyrate Metabolism in Tg PD-ABAD Mice—Tg PD-ABAD and control mice were infused with D-[2,4-^{13}C]3-hydroxybutyrate. ^{13}C NMR spectra of cerebral cortical extracts from Tg PD-ABAD and non-Tg littermate control (the latter spectra are not shown) mice illustrate labeling of glutamate and glutamine in the C-4, C-3, and C-2 positions, as well as GABA in the C-2 position (Fig. 7*A*), consistent with entry of [^{13}C]β-hydroxybutyrate via 2-[^{13}C]acetyl-CoA into the tricarboxylic acid cycle. The intensity of glutamate and glutamine C-4 resonance was 50 and 20% greater, respectively, in Tg PD-ABAD mice compared with non-Tg littermates (Fig. 7*B*). The glutamate to glutamine ratio, based on C-4 resonance area, was 3.6 ± 0.3 in non-Tg *versus* 2.1 ± 0.4 in Tg PD-ABAD mouse brains ($p < 0.03$). These data suggest that glutamine synthesis is more efficient in Tg PD-ABAD mouse brain compared with controls. The area of the ^{13}C-labeled C-2 resonance of GABA was also greater in Tg PD-ABAD mice (4.8 ± 0.3) than in non-Tg controls (2.2 ± 0.5; $p < 0.04$). Such increased labeling of GABA is consistent with enhanced conversion of labeled glutamate to GABA in brains of Tg mice. ^{1}H NMR analysis of these extracts revealed that the fractional enrichment in glutamate C-4 was significantly greater in Tg PD-ABAD (58 ± 5%) than in non-Tg littermates (38 ± 7%; $p < 0.03$). As might be expected from the increased utilization of exogenous β-hydroxybutyrate, measurement of basal ATP levels in cerebral

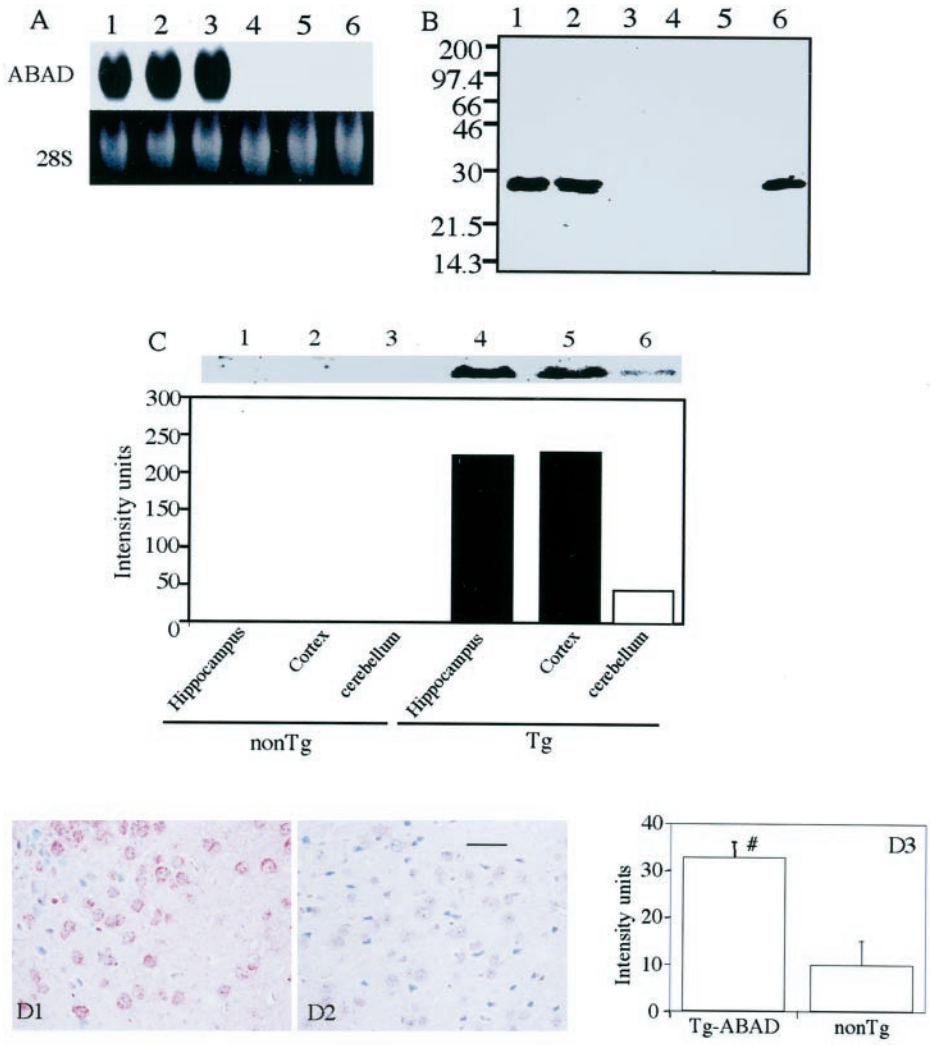

FIG. 6. **Characterization of Tg PD-ABAD mice.** *A*, Northern analysis for ABAD transcripts in cerebral cortex from mice representing three different lines of Tg PD-ABAD animals (*lanes 1–3*) and three nontransgenic littermate controls (*lanes 4–6*). Cerebral cortex was harvested from 3–4-month-old mice, and total RNA was prepared, subjected to electrophoresis on agarose (5%) gels (30 μg of RNA was added to each lane) followed by transfer to membranes and hybridization with ^{32}P-labeled ABAD cDNA (RNA loading was estimated by ethidium bromide staining of the 28S ribosomal RNA band). *B*, Western analysis was performed on protein extracts from cerebral cortex of mice representing three lines of Tg PD-ABAD animals (*lanes 1*, *2*, and *6*) and from three nontransgenic littermate controls (*lanes 3–5*). Cerebral cortex was harvested from 3–4-month-old mice, and protein extracts were prepared and subjected to SDS polyacrylamide gel electrophoresis (12%; reduced; 100 μg of protein was added to each lane)/immunoblotting with anti-ABAD IgG (10 μg/ml). *C*, immunoblotting was performed on the indicated brain subregion of one Tg PD-ABAD mouse using anti-human ABAD peptide IgG with 100 μg of total protein extract loaded in each case (this antibody does not react with endogenous ABAD murine epitopes). Representative results are shown with a mouse from one line of Tg PD-ABAD mice, and these experiments were repeated three times with different mice from the same line of Tg PD-ABAD animals. *D*, immunohistochemical study of cerebral cortex from the brain of a Tg PD-ABAD mouse (*D1*) with anti-human ABAD peptide IgG (10 μg/ml) displaying the presence of the antigen in cortical neurons compared with a non-Tg control mouse (*D2*). *D3*, semiquantitative analysis of immunohistochemical results in Tg PD-ABAD and non-Tg littermate controls as described in the text.

cortex of Tg PD-ABAD mice fasted overnight showed a statistically significant increase compared with non-Tg littermates (Fig. 7*C*). Similarly, levels of β-hydroxybutyrate in the brains of Tg PD-ABAD mice were lower, compared with non-Tg controls (Fig. 8*D*). This is consistent with increased utilization of β-hydroxybutyrate in the presence of higher levels of neuronal ABAD.

Induction of Stroke in Tg PD-ABAD Mice—To assess the possible contribution of ABAD to ischemic stress, Tg PD-ABAD and age-matched non-Tg littermate control mice were subjected to a 45-min period of transient middle cerebral artery occlusion followed by a 24-h period for evolution of the cerebral infarct. These studies utilized a protocol that we have found to provide reproducible stroke volumes and functional data (neurologic deficit scores, cerebral blood flow) (45–48). Levels of ABAD increased an additional ~2-fold in Tg PD-ABAD mice after stroke, *versus* with untreated/control Tg PD-ABAD mice. Compared with non-Tg littermate controls, Tg PD-ABAD mice displayed strokes of smaller volume and lower neurologic deficit scores (consistent with better maintenance of neurologic function) (Fig. 8, *A* and *B*). In contrast, there was no change in cerebral blood flow comparing the Tg and non-Tg animals (not shown), consistent with a direct effect of ABAD on neurons, as ABAD was overexpressed in neurons by the PDGF B-chain promoter. Analysis of cerebral cortex from Tg animals showed increased ATP and decreased lactate levels compared with non-Tg controls (Fig. 8*C*). In addition, β-hydroxybutyrate levels were lower in animals subjected to cerebral ischemia, and this finding was much more pronounced in Tg PD-ABAD mice compared with non-Tg littermate controls (Fig. 8*D*). These data

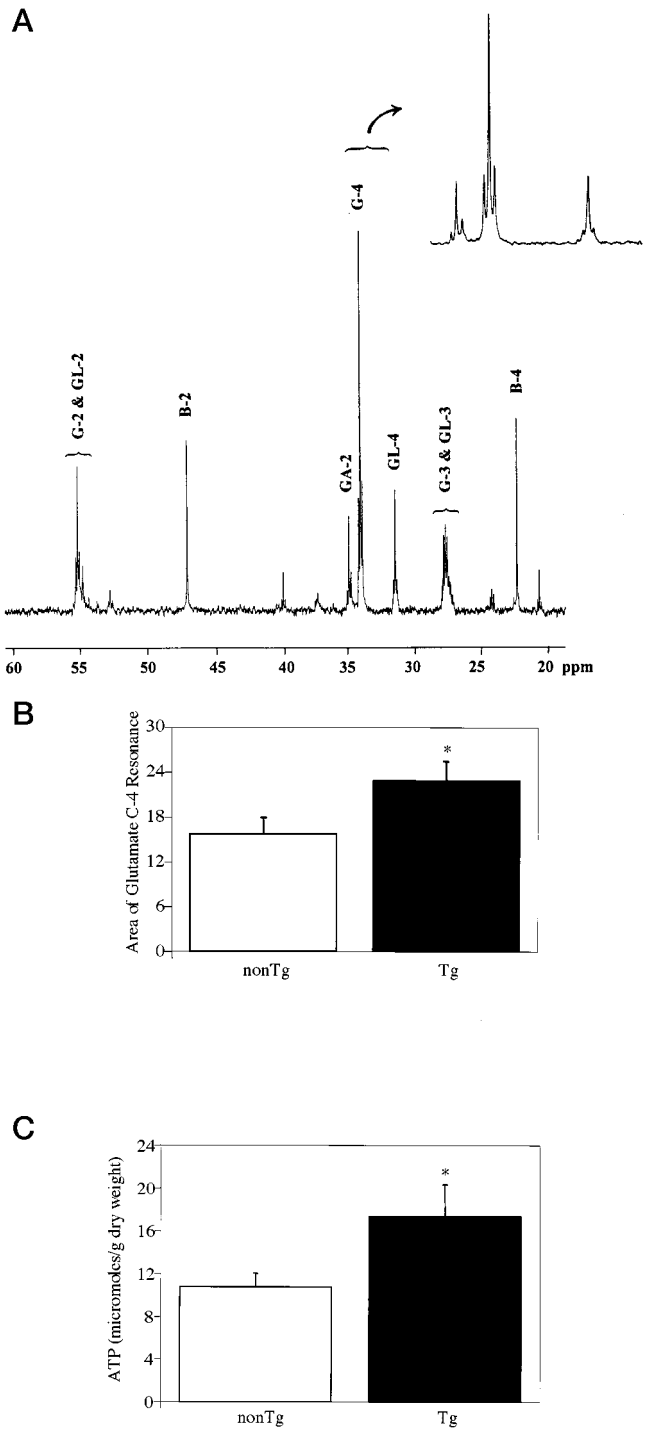

FIG. 7. **The effect of ABAD overexpression on the proton-decoupled ^{13}C NMR spectra of freeze-clamped brain after perfusion with D-[2,4-^{13}C]β-hydroxybutyrate.** *A*, the spectrum from a representative Tg PD-ABAD mouse displays prominent glutamate and glutamine peaks. The *inset* shows expanded regions of resonances of glutamate (G-4), glutamine (GL-4), and GABA (GA-2) from Tg (PD-ABAD) mice. *G-2*, *G-3*, and *G-4* denote the position 2, 3, and 4 carbons of glutamate, respectively; *GL-2*, *GL-3*, and *GL-4* denote the position 2, 3, and 4 carbons of glutamine, respectively; and *GA-2* corresponds to C-2 of GABA. *B*, the effect of ABAD overexpression on areas of glutamate C-4 resonance in brain extracts of Tg PD-ABAD and non-Tg littermate control mice as obtained from ^{13}C NMR analysis. Values are expressed as the ratio of the area of the glutamate C-4 peak over the area of an added standard acetate (see "Materials and Methods"). The *asterisk* indicates glutamate and glutamine levels significantly higher in Tg PD-ABAD mice than in non-Tg controls ($p < 0.03$; $n = 4$, in each case). Total areas of [^{13}C]glutamate (G-2 + G-3 + G-4) were significantly higher in the Tg PD-ABAD compared with nonTG littermate controls. *C*, basal ATP levels in whole brain extracts from Tg PD-ABAD ($n = 5$) or non-Tg littermate controls ($n = 5$) were measured as described in the text. Animals were fasted overnight, and the brain was removed and freeze-clamped for ATP and β-hydroxybutyrate analysis. The *asterisk* indicates $p < 0.03$. In each case, the data are reported as the means ± S.D.

suggested better maintenance of energy reserve and substrate metabolism in Tg PD-ABAD mice subjected to ischemia.

DISCUSSION

ABAD is a member of the short chain dehydrogenase/reductase family with remarkably broad substrate specificity, now extended to include the ketone body D-β-hydroxybutyrate. In comparison with mitochondrial D-β-hydroxybutyrate dehydrogenase (52–55), which displays a K_m ~1 mM, ABAD displays a K_m of ~4.5 mM. At β-hydroxybutyrate concentrations in the plasma of normal individuals (<1 mM), both enzymes would be working considerably below their respective K_m values. Under pathologic conditions, when β-hydroxybutyrate concentrations can reach the millimolar range (21–23), both enzymes would be expected to metabolize β-hydroxybutyrate. However, the maximal activity of ABAD with D-β-hydroxybutyrate (0.0039 μmol/min/mg) is much lower than that for the mitochondrial enzyme (V_{max} = ~100–175 μmol/min/mg protein with β-hydroxybutyrate) (54, 55). D-β-Hydroxybutyrate dehydrogenase is a housekeeping metabolic enzyme present in mitochondria whose expression has not been reported to vary in pathologic states, beyond its loss from severely ischemic cardiac tissue (56, 57). ABAD, present in both endoplasmic reticulum and mitochondria, displays a pattern of expression sensitive to environmental perturbations, including increased expression in brains of patients with Alzheimer's disease (13) and at sites of ischemic brain injury (Fig. 5). Thus, in settings where ABAD expression is enhanced, the enzyme could, potentially, contribute to the metabolism of β-hydroxybutyrate. However, the situation is likely to be more complex *in vivo*, because Tg PD-ABAD mice display increased flux of acetyl-CoA through the tricarboxylic acid cycle and higher ATP levels in the cerebral cortex, even though the level of ABAD expression is only increased by about 3.5–4-fold, compared with nontransgenic controls. These data indicate that ABAD clearly has the potential to contribute to β-hydroxybutyrate metabolism, although the extent of its contribution is likely to depend on the particular situation.

Increased expression of ABAD in human brain following cerebral infarction[2] and in response to experimentally induced cerebral ischemia (Fig. 5) suggests that induction of ABAD might subserve normal protective mechanisms. In view of the complexities of cellular metabolic pathways, it was necessary to prove that ABAD could promote metabolic homeostasis in response to nutritional deprivation. ABAD-transfected COS cells displayed increased energy charge and flux of acetyl-CoA through the tricarboxylic acid cycle in medium containing β-hydroxybutyrate compared with controls in which the active site of ABAD was mutationally inactivated. Enhanced metabolic homeostasis was reflected by maintenance of MTT reduction and morphologic phenotype in ABAD-transfected COS cells. Similarly, transgenic mice overexpressing ABAD in cortical neurons demonstrated increased flux of acetyl-CoA through the tricarboxylic acid cycle following β-hydroxybutyrate infusion compared with nontransgenic littermates. However, increased basal levels of ATP (and energy charge; data not shown) in brains of Tg PD-ABAD mice, even before nutritional stress,

[2] S.-D. Yan and D. Stern, unpublished observations.

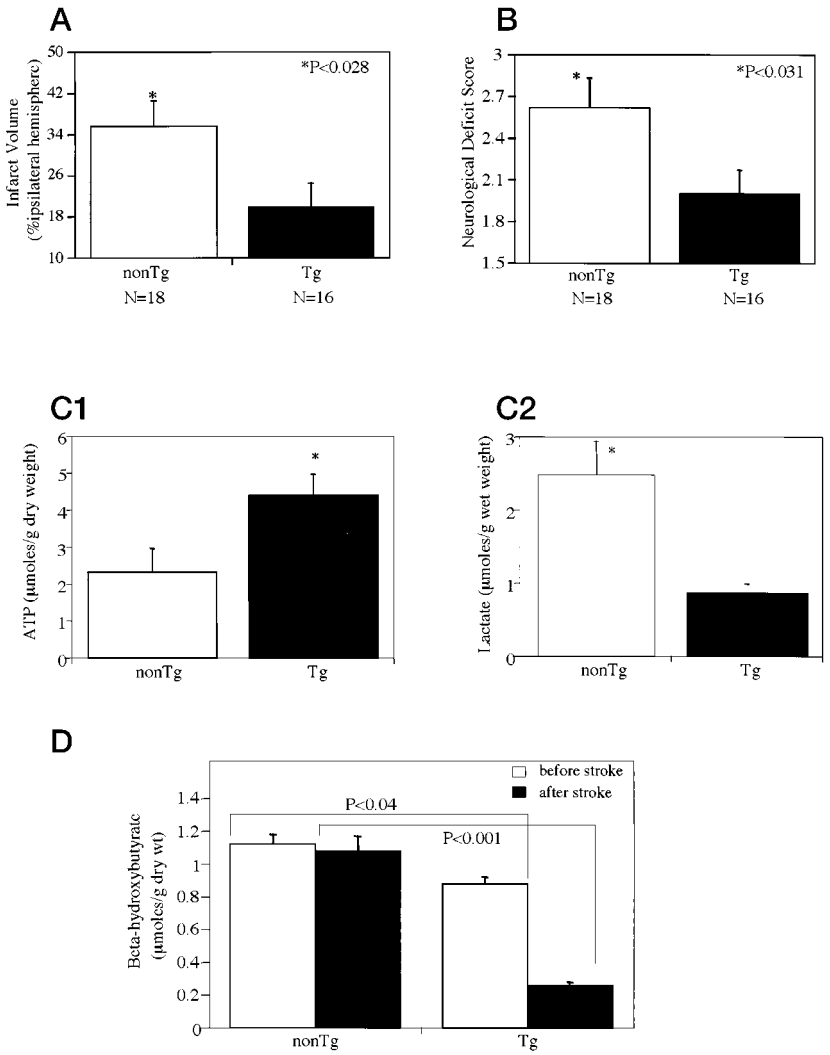

FIG. 8. **Induction of stroke in Tg PD-ABAD mice.** *A* and *B*, Tg PD-ABAD mice and non-Tg littermates were subjected to middle cerebral artery occlusion and were evaluated 24 h after the ischemic insult to determine neurologic deficit score (*B*) and, following sacrifice, infarct volume (*A*). *C* and *D*, at the same time point, cerebral cortex was harvested to determine ATP, lactate, and β-hydroxybutyrate levels determined on extracts of whole brains (from animals subjected to the stroke procedure 24 h previously) from Tg PD-ABAD or non-Tg control mice ($n = 5$, in each case). Data are reported as the means.

were unexpected and suggest a more general protective potential of ABAD in response to a range of environmental challenges. This apparent increase in the overall energy charge in the presence of ABAD implies that the enzyme may render neurons metabolically more stable and, thus, less susceptible to fluctuations in substrate availability.

A decreased lactate content in the cerebral cortex of Tg PD-ABAD mice subjected to stroke suggests two important events associated with neuroprotection. First, decreased tissue lactate and lower lactate/pyruvate ratio in the Tg PD-ABAD mice are indicative of diminished cytosolic NADH/NAD^+ ratio and consistent with decreased reductive stress. In this context, studies have suggested that diminished in reductive stress may translate into lower reactive oxygen species generation upon reperfusion (58). Second, decreased tissue lactate is also indicative of efficient lactate efflux in stroke-prone tissue, thereby alleviating feedback inhibition brought about by metabolic intermediates of glycolysis (59–61).

Our NMR measurements were based on conversion of α-ketoglutarate, an intermediate in the tricarboxylic acid cycle, to glutamate. However, we also observed conversion of glutamate, thus formed, to glutamine and GABA. These data indicate that ketone bodies, such as β-hydroxybutyrate, can provide both a substrate for maintenance for cellular energy charge, as well as a source for increased production of neurotransmitters. To our knowledge, this is the first time that the conversion of labeled β-hydroxybutyrate to GABA and glutamate has been demonstrated *in vivo*. Furthermore, the increased production of ^{13}C-labeled GABA and glutamate from [^{13}C]β-hydroxybutyrate in Tg PD-ABAD mice, compared with controls, indicates that ABAD provides a novel means for sustaining energy production and replenishing neurotransmitters in the brain using ketone bodies as the substrate. At this point, it is unclear whether neuroprotection afforded by overexpression of ABAD is due solely to its effect on ATP levels and/or changes in neurotransmitter metabolism.

In contrast to this cytoprotective facet of ABAD biology, we have proposed that in the presence of Aβ, another, quite different, aspect of the properties of ABAD becomes manifest (14). In an Aβ-rich environment, ABAD generates reactive oxygen intermediates and toxic reactive aldehydes based on cotransfection experiments using cultured COS and neuroblastoma cells (14).[2] Furthermore, pilot studies with double transgenic mice, resulting from a cross of Tg PD-ABAD mice with transgenic mice overexpressing mutant βAPP, have shown accelerated expression of cell stress markers (4-hydroxynonenal and heme oxygenase type 1), compared with single transgenic mice, and nontransgenic controls.[2] Based on these data, ABAD appears to have chameleon-like properties depending on the local environment, in particular related to the presence of Aβ. Our future studies have the goal of determining how the properties of ABAD become modulated in an Aβ-rich environment and whether this translates into accelerated and more severe neuronal dysfunction/toxicity. The current studies provide a foundation for evaluating metabolic properties of ABAD in response to cellular stress *in vitro* and *in vivo*.

REFERENCES

1. Hardy, J. (1997) *Trends Neurosci.* **296,** 28570–26998
2. Citron, M., Westaway, D., Xia, W., Carlson, G., Diehl, T., Levesque, G., Johnson-Wood, K., Lee, M., Seubert, P., Davis, A., Kholodenko, D., Motter, R., Sherrington, R., Perry, B., Yao, H., Strome, R., Lieberburg, I., Rommens, J., Kim, S., Schenk, D., Fraser, P., St. George-Hyslop, P., and Selkoe, D. (1997) *Nat. Med.* **3,** 67–72
3. St. George-Hyslop, P (1998) *Neurobiol. Aging* **19,** 133–137
4. Selkoe, D. (1999) *Ann. Rev. Cell Biol.* **10,** 373–403
5. Liao, A., Nitsch, R., Greenberg, S., Finckh, U., Blacker, D., Albert, M., Rebeck, G., Gomez-Isla, T., Clatworthy, A., Binetti, G., Hock, C., Mueller-Thomsen, T., Mann, U., Zuchowski, K., Beisiegel, U., Staehelin, H., Growdon, J., Tanzi, R., and Hyman, B. (1998) *Human Mol. Gen.* **12,** 1953–1956
6. Kisilevsky, R., Lemieux, J., Fraser, P., Kong, X., Hultin, P., and Szarek, W. (1995) *Nat. Med.* **1,** 143–148
7. Goldgaber, D., Schwarzman, A., Bhasin, R., Gregori, L., Schmechel, D., Saunders, A. M., Roses, A. D., and Strittmatter, W. J. (1993) *Ann. N. Y. Acad. Sci.* **695,** 139–143
8. Roses, A. (1998) *Ann. N. Y. Acad. Sci.* **855,** 738–743
9. Hensley, K., Carney, J. M., Mattson, M. P., Aksenova, M., Harris, M., Wu, J. F., Floyd, R. A., and Butterfield, D. A. (1994) *Proc. Natl. Acad. Sci. U. S. A.* **91,** 3270–3274
10. Mattson, M., and Goodman, Y. (1995) *Brain Res.* **676,** 219–224
11. Mark, R., Blanc, E., and Mattson, M. (1996) *Mol. Neurobiol.* **12,** 915–924
12. Mattson, M. (1995) *Neurobiol. Aging* **16,** 679–682
13. Yan, S. D., Fu, J., Soto, C., Chen, X., Zhu, H., Al-Mohanna, F., Collison, K., Zhu, A., Stern, E., Saido, T., Tohyama, M., Ogawa, S., Roher, A., and Stern, D. (1997) *Nature* **389,** 689–695
14. Yan, S-D., Shi, Y., Zhu, A., Fu, J., Zhu, H., Zhu, Y., Gibson, L., Collison, K., Al-Mohanna, F., Ogawa, S., Roher, A., Clarke, S., and Stern, D. M. (1998) *J. Biol. Chem.* **274,** 2145–2156
15. Jornvall, H., Persson, B., Krook, M., Atrian, S., Duarte-Gonzalez, R., Jeffer, J., and Ghosh, D. (1995) *Biochemistry* **34,** 6003–6013
16. Furuta, S., Kobayashi, A., Miyazawa, S., and Hashimoto, T. (1997) *Biochim. Biophys. Acta* **1350,** 317–324
17. Kobayashi, A., Jiang, L., and Hashimoto, T. (1996) *J. Biochem.* (*Tokyo*) **119,** 775–782
18. He, X.-Y., Schulz, H., and Yang, S.-Y. (1998) *J. Biol. Chem.* **273,** 10741–10746
19. He, X-Y., Merz, G., Mehta, P., Schulz, H., and Yang, S.-Y. (1999) *J. Biol. Chem.* **274,** 15014–15019
20. Torroja, L., Ortuno-Sahagun, D., Ferrus, A., Hammerle, B., and Barbas, J. (1998) *J. Cell Biol.* **141,** 1009–1017
21. Levitsky, L., Fisher, D., Paton, J., and Delannoy, C. (1977) *Pediatr. Res.* **11,** 298–302
22. Owen, O., Morgan, A., Kemp, H., Sullivan, J., Herrera, M., and Cahill. G. (1967) *J. Clin. Invest.* **46,** 1589–1595
23. Petersson, B., Settergren, G., and Dahlquist, G. (1972) *Acta Paediat. Scand.* **61,** 273–277
24. Segel, I. H. (1975) *Enzyme Kinetics, Behavior, and Analysis of Rapid Equilibrium and Steady-State Enzyme Systems*, Wiley-Interscience, New York
25. Johnson, D., Gautsch, J., Sportsman, J., and Elder, J. (1984) *Gene Anal. Tech.* **1,** 3–8
26. Schmidt, A. M., Vianna, M., Gerlach, M., Brett, J., Ryan, J., Kao, J., Esposito, C., Hegarty, H., Hurley, W., Clauss, M., Wang, F., Pan, Y. C., Tsang, T. C., and Stern, D. M. (1992) *J. Biol. Chem.* **267,** 14987–14997
27. Schmidt, A. M., Hori, O., Brett, J., Yan, S. D., Wautier, J. L., and Stern, D. M. (1994) *Arterioscler. Thromb.* **14,** 1521–1528
28. Kuwabara, K., Matsumoto, M., Ikeda, J., Ogawa, S., Maeda, Y., Kitagawa, K., Imuta, N., Kinoshita, T., Stern, D., Yangi, H., and Kamada, T. (1996) *J. Biol. Chem.* **271,** 5025–5032
29. Du, Y., Dodel, R., Bales, K., Jemmerson, R., Hamilton-Byrd, E., and Paul, S. (1997) *J. Neurochem.* **69,** 1382–1388
30. Sonnewald, U., Westergaard, N. Hassel, B., Muller, T., Unsgard, G., Fonnum, F., Hertz, L., Schousboe, A., and Petersen, S. (1993) *Dev. Neurosci.* **15,** 351–358
31. Badar-Goffer, R., Bachelard, H., and Morris, P. (1990) *Biochem. J.* **266,** 133–139
32. Jones, J., Hansen, J., Sherry, A., Malloy, C., and Victor, R. (1997) *Anal. Biochem.* **249,** 201–206
33. London, R. (1988) *Prog. NMR Spectroscopy* **20,** 337–383
34. Malloy, C., Sherry, A., and Jeffrey, F. (1987) *FEBS Lett.* **212,** 58–62
35. Trueblood, N., and Ramasamy, R. (1998) *Am. J. Physiol.* **275,** H75–H83
36. Chatham, J. C., Forder, J. R., Glickson, J. D., and Chance, E. M. (1995) *J. Biol. Chem.* **270,** 7999–8008
37. Jeffrey, F., Diczku, V., Sherry, A., and Malloy, C. (1995) *Basic Res. Cardiol.* **90,** 388–396
38. Fitzpatrick, S., Hetherington, H., Behar, K., and Shulman, R. (1990) *J. Cereb. Blood Flow Metab.* **10,** 170–179
39. Behl, C., Davis, J., Lesley, R., and Schubert, D. (1994) *Cell* **77,** 817–827
40. Imuta, N., Ogawa, S., Maeda, Y., Kuwabara, K., Hori, O., Ueda, H., Tanagihara, T., and Tohyama, M. (1998) *J. Neurochem.* **70,** 550–557
41. Ueda, H., Hashimoto, T., Furuya, E., Tagawa, K., Kitagawa, K., Matsumoto, M., Yoneda, S., Kimura, K., and Kamada, T. (1988) *J. Biochem.* (*Tokyo*) **104,** 81–86
42. Sasahara, M., Fries, J., Raines, E., Gown, A., Westrum, L., Frosch, M., Bonthron, D., Ross, R., and Collins, T. (1991) *Cell* **64,** 217–227
43. Kang, D., Soriano, S., Frosch, M., Collins, T., Naruse, S., Sisodia, S., and Koo, E. (1999) *J. Neurosci.* **19,** 4229–4237
44. Berezovska, O., Frosch, M., McLean, P. Knowles, R., Koo, E., Kang, D., Lu, F., Lux, S., Shen, J., Onegawa, S., Hyman, B., (1999) *Brain Res. Mol. Brain Res.* **69,** 273–280
45. Huang, J., Kim, L., Mealey, R., March, H., Zhang, A., Tenner, E., Connolly, E., and Pinsky, D. (1999) *Science* **285,** 595–599
46. Connolly, E. S., Winfree, C. J., Stern, D. M., Solomon, R. A., and Pinsky, D. J. (1996) *Neurosurgery* **38,** 523–532
47. Connolly, E., Winfree, C., Springer, T., Naka, Y., Liao, H., Yan, S.-D., Stern, D., Solomon, R., Gutierrez-Ramos, J.-C., and Pinsky, D. (1996) *J. Clin. Invest.* **97,** 209–216
48. Connolly, E., Winfree, C., Prestigiacomo, C., Kim, S., Choudhri, T., Hoh, B., Naka, Y., Solomon, R., and Pinsky, D. (1997) *Circ. Res.* **81,** 304–310
49. Bederson, J. B., Pitts, L. H., and Tsuji, M. (1986) *Stroke* **17,** 472–476
50. Sellevold, O., Jynge, P., and Aarstad, K. (1986) *J. Mol. Cell. Cardiol.* **18,** 517–527
51. Lamprecht, W., and Heinz, F. (1995) *Method of Enzymatic Analysis*, Verlag Chemie, Boca Raton, FL
52. McCann, W. (1957) *J. Biol. Chem.* **226,** 15–22
53. Lehninger, A., Sudduth, H., and Wise, J. (1960) *J. Biol. Chem.* **235,** 2450–2455
54. Bock, H., and Fleischer, S. (1975) *J. Biol. Chem.* **250,** 5774–5781
55. McIntyre, J., Latruffe, N., Brenner, S., and Fleischer, S. (1988) *Arch. Biochem. Biophys.* **262,** 85–98
56. Evertsen, F., Medbo, J., Jebens, E., and Gjovaag, T. (1999) *Acta Physiol. Scand.* **167,** 247–257
57. Frederiks, W., Tukkie, R., Grundeman, P., and Schellens, J. (1995) *J. Pathol.* **175,** 339–348
58. Williamson, J., Chang, K., Frangos, M., Hasan, K., Ido, Y., Kawamura, T., Nyengaard, J., Van den Enden, M., Kilo, C., and Tilton, R. (1993) *Diabetes* **42,** 801–813
59. Neely, J., and Morgan, H. (1974) *Annu. Rev. Physiol.* **36,** 413–459
60. King, L., and Opie, L. (1998) *Mol. Cell. Biochem.* **180,** 3–26
61. Lipton, P. (1999) *Physiol. Rev.* **79,** 1431–1568